Hindawi
Mathematical Problems in Engineering
Volume 2020, Article ID 8835267, 16 pages
https://doi.org/10.1155/2020/8835267

Research Article

Robust Design Optimization of Car-Door Structures with Spatially Varied Material Uncertainties

Yuee Zhao,[1] **Hai Dong**,[1] **and Haibin Liang**[2]

[1]*School of Applied Technology, Shenyang University, Shenyang, Liaoning 110044, China*
[2]*Application Engineering Center, Weichai Power Co., Ltd., Jinan, Shandong 261061, China*

Correspondence should be addressed to Hai Dong; sydxhd@foxmail.com

Received 25 September 2020; Revised 29 October 2020; Accepted 31 October 2020; Published 16 November 2020

Academic Editor: Shun-Peng Zhu

This paper presents an effective approach for robust design optimization of car-door structures with spatially varied material properties. This spatially varied material property causes structural response quantities; for example, the natural frequency and the lateral stiffness coefficient become random variables. In this regard, the Karhunen-Loève expansion is first used to represent the elastic modulus and the mass density random fields as a series of random variables. Then, a stochastic finite-element model is formulated for uncertainty quantification of the car-door structure. Combined with a polynomial-based response surface model to mimic the true performance indicator, this allows one to efficiently evaluate probability constraints for the robust design optimization of the uncertain car-door structure. In numerical simulations, design variables of the uncertain car-door structure are defined as thickness values of the tailor rolled blank structure at various regions, whereas multiple design objectives are formulated via the structural weight, the first-order natural frequency, and the lateral stiffness coefficient. Results have shown that the mean value of performance indicators can be generally improved, whereas the response variance is further minimized to archive the robust design objective. The probability-based constraint is significant to relate the Pareto optimum set to the targeted structural safety level. The proposed approach is simple, suggesting an attractive tool for the robust design optimization of car-door structures with spatially varied material uncertainties.

1. Introduction

The design optimization of car-door structures has received considerable attention due to its significant role in the daily safe commuting of students [1, 2]. In this regard, Kunakornong et al. [3] realized the design optimization of bus structures by considering Sandwich composite via the finite-element approach. Lan et al. [4] presented the comparative design optimization of bus side structures with and without supporting members between longitudinal beams, whereas the multiobjective design optimization of bus structures was considered in Zhong et al. [5] to simultaneously minimize the structural total weight and maximize the torsional stiffness. Together with the lightweight design objective, performance indicators are formulated as the structural lateral stiffness and the first-order natural frequency in this paper. Specifically, probability constraints to evaluate the exceeding probability of the two performance indicators over their design limits are further considered to account for structural safety concerns.

Numerical iterations for design optimization of the car-door structure are usually realized based on a finite-element (FE) model that depicts the structural implicit function, for example, the first-order natural frequency and the lateral stiffness coefficient. The gradient-based optimization algorithm, however, needs to recursively run the FE model for optimum design variables [6, 7]. This is computationally demanding for the design optimization involving high-dimensional input parameters. Many surrogate modelling algorithms, for example, the Gaussian process regression method [8], the polynomial chaos expansion, and the artificial neural networks, were considered in the literature [9, 10]. Once a response surface model that mimics the true performance function is analytically or numerically

available, the Pareto optimal set can be obtained for the lightweight and the dynamic/strength design optimization of the car-door structure.

Another issue is about various sources of input uncertainties associated with the structural simulation model, for example, the geometry, the material property, and the loading parameters [11]. Take the elastic modulus and the mass density car-door structure as examples, which are actually realized as the high-strength alloy steel. This material property might show spatially varied uncertainties due to fluctuated manufacturing factors, for example, the pressure, the temperature, and the milling force. This motivates us to employ the random field theory for structural uncertainty simulation [12]. This is because the optimum obtained via the deterministic model sometimes becomes unrealistic and less meaningful in reality [13]. Along with various contributions of the deterministic optimization in the literature [14, 15], this paper considers optimizing the structural performance and minimizing the response variance, that is, the robust-based design optimization of car-door structures with uncertain input factors.

In general, a realization of the spatially varied material property consists of an infinite number of random variables, which occur explicitly in the structural governing equation [16]. After considering the safety constraint for highly reliable structures, the spatially varied input uncertainty cannot be directly handled by ordinary simulation algorithms [17, 18]. The uncertainty quantification of the uncertain car-door structure, hence, becomes a challenging but highly demanding task [19]. To address the spatially varied input uncertainty, the Karhunen-Loève (K-L) expansion is used to represent the material random field as a small number of deterministic functions and independent random variables [20]. This is useful to develop a stochastic FE model for uncertainty simulation of the car-door structure.

Once a simulation model is set up to depict the implicit design performance function of the car-door structure, the multiple design objectives can be numerically optimized via a global iteration algorithm [21], for example, the genetic algorithm in this paper. Therefore, the dynamic characteristics of the car-door structure are first modelled by the FE formulation and the Mindlin plate theory [22–24]. Herein, the stochastic stiffness and mass formulations are determined based on the numerical results of the material random field. Note that the material property has been subjectively assumed as deterministic constants, which implies that the Gauss-Legendre scheme with three to six points can be used to evaluate the stiffness and mass integrals. The introduction of the spatially varied random field, however, results in high-order eigenfunctions to define the stochastic FE matrix, and high-order Gauss-quadrature schemes are required to address the multivariate integration problem. Specifically, the FE model becomes stochastic due to input random variables associated with the material random field. This motivates the robust design optimization to minimize the structural response variance. Note that other advanced plate models can be alternatively used to perform a numerical simulation of the car-door structure. The presented stochastic FE model and the robust design method are general to determine the corresponding design optimization results.

The objective of this manuscript is to present an effective approach for the robust design optimization of car-door structures with spatially varied material uncertainties. To begin with, the elastic modulus and the mass density of the car-door structure are modelled as the Gaussian random field, which is numerically represented through the K-L expansion method with a small number of deterministic spatial functions and Gaussian random variables. Then, a stochastic FE model for structural uncertainty analysis is set up based on the simulated material random field and the Mindlin plate theory. This allows one to numerically determine stochastic samples for uncertain analysis, for example, the natural frequency and the lateral stiffness coefficient of the car-door structure. To reduce the computational cost for recursively running the stochastic FE model, a polynomial-based response surface is used to mimic the true design performance function. The robust design objective is formulated via the structural lightweight indicator, the first-order natural frequency, and the lateral stiffness coefficient. Note that the minimization of the response variance has been taken into account to search for robust design solutions. Together with structural safety constraints in terms of the nonexceeding probability with respect to the natural frequency and the lateral stiffness, the Pareto optimum set is obtained for robust design optimization car-door structures with spatially varied material uncertainties.

The rest of this manuscript is organized as follows. Section 2.1 briefly summarizes the K-L expansion method for numerical representation of material random fields, whereas simulation results for the elastic modulus and the mass density random fields are demonstrated in Section 2.2. In Section 3, the stochastic finite-element model for structural uncertainty simulation is further developed. This is used to define multiple design objectives and safety constraints in Section 4.1. To reduce computational cost caused by recursively running the stochastic FE model, a polynomial-based response surface model is presented in Section 4.2 to mimic the true design performance indicator. Combined with the genetic algorithm to search for the global optima, the Pareto sets are determined in Section 4.3 for various structural safety levels. Conclusions are summarized in Section 5.

2. Uncertain Modelling of Spatially Varied Material Properties

To model spatially varied material properties of the car-door structure, this section first briefly summarizes the K-L expansion method. Numerical simulation results for the mass density and Young's modulus random fields are followed to demonstrate the engineering applications. Due to the spatially varied material uncertainty, the structural response quantity, for example, the first-order natural frequency or the lateral stiffness coefficient, becomes a random variable. This motivates the robust design optimization to minimize the response variance of the car-door structure. To begin

with, the numerical representation of the material random field is presented based on the K-L expansion method as follows.

2.1. The Karhunen-Loève Expansion. The section considers the numerical representation of a two-dimensional material random field $H(x, y; \xi)$. A sample of the spatially varied material property contains infinity numbers of random variables. This motivates the utility of the K-L expansion method to represent the random field by means of random variables.

Following the random field theory, the expectation of the two-dimensional material random field is defined as

$$\mu_H(x, y) = \int_D H(x, y; \boldsymbol{\xi}) \mathrm{d}\boldsymbol{\xi}, \tag{1}$$

and $H'(x, y; \xi) = H(x, y; \xi) - \mu_H(x, y)$ denotes the fluctuation of $H(x, y; \xi)$ with respect to the mean-value function. Therefore, the covariance function of the material random field is defined as

$$\mathrm{Cov}(x, x'; y, y') = E[H'(x, y; \boldsymbol{\xi}) H'(x, y; \boldsymbol{\xi})], \tag{2}$$

which is a nonnegative quantity for any function $\phi(x, y)$ on a subregion $\Omega_e \subseteq \Omega$:

$$\sum_{x,x',y,y' \in \Omega_e} \mathrm{Cov}(x, x'; y, y') \phi(x, y) \phi(x', y') > 0. \tag{3}$$

Through the K-L expansion method, the two-dimensional random field $H(x, y; \xi)$ can be represented as [25]

$$HH(x, y; \boldsymbol{\xi}) = \mu_H(x, y) + \sum_{i=1}^{\infty} \sqrt{\lambda_i} \phi_i(x, y) \xi_i, \tag{4}$$

where $\mu_H(x, y)$ represents the mean value of the random field and the eigenvalues λ_i and eigenfunctions $\phi_i(x, y)$ are the solution of the two-dimensional homogeneous Fredholm integral equation of the second kind [26]:

$$\int_\Omega \mathrm{Cov}(x, x'; y, y') \phi(x, y) \mathrm{d}x \mathrm{d}y = \lambda \phi(x', y'). \tag{5}$$

Specifically, arbitrary two orders of the eigenfunction are orthogonally defined with respect to each other; that is, $\int_\Omega \phi_i(x, y) \phi_j(x, y) \mathrm{d}x \mathrm{d}y = \delta_{ij}$, where δ_{ij} is the Kronecker symbol. This determines uncorrelated random variables ξ_i as

$$\xi_i = \frac{1}{\sqrt{\lambda_i}} \int_\Omega H'(x, y; \boldsymbol{\xi}) \phi_i(x, y) \mathrm{d}x \mathrm{d}y, \tag{6}$$

and the eigendecomposition of the covariance model is given as

$$\mathrm{Cov}(x, x'; y, y') = \sum_{i=1}^{\infty} \lambda_i \phi_i(x, y) \phi_i(x', y'), \tag{7}$$

which contains infinity orders of the eigensolution $\{\lambda_i, \phi_i(x, y)\}$.

After truncating the K-L expansion after M terms, an approximation of the two-dimensional material random field $H(x, y; \xi)$ is given as

$$\widehat{H}(x, y; \boldsymbol{\xi}) = \mu_H(x, y) + \sum_{i=1}^{M} \sqrt{\lambda_i} \phi_i(x, y) \xi_i, \tag{8}$$

which is approximated by M-order eigenfunctions and the corresponding Gaussian random variables $\xi_i (i = 1, \ldots, M)$.

Numerical simulation of the random field needs to solve the integral eigenvalue problem (IEVP) in equation (6), and the analytic solution is seldom available except for a few covariance models defined on canonical regions, for example, the rectangular and circles in the two-dimensional case. One has to resort to a numerical algorithm, for example, the collocation or the expansion optimal linear estimation (EOLE) method in the literature [27].

Once numerical results for the eigensolution $\{\lambda_i, \phi_i(x, y)\}$ are derived, a realization of the two-dimensional material random field can be given as

$$\widehat{H}(x, y; \boldsymbol{\xi}) = \mu_H(x, y) + \sum_{i=1}^{M} \sqrt{\widehat{\lambda}_i} \widehat{\phi}_i(x, y) \xi_i, \tag{9}$$

where $\{\widehat{\lambda}_i, \widehat{\phi}_i(x, y)\}$ denote numerical solutions of the true but unknown eigenpairs, which are numerically determined via the high-order polynomial-based Ritz-Galerkin approximation approach [28]. The corresponding simulation results of the two-dimensional material random field are further presented as follows.

2.2. Numerical Realizations of the Material Random Field. To demonstrate the utility of the K-L expansion method for numerical representation of spatially varied material uncertainties, this section presents simulation results for the elastic modulus random field of the car-door structure. To begin with, Figure 1 depicts the structural simulation domain, which has been discretized via 1028 Q4 elements. Note that this random field simulation algorithm can deal with other structural geometries once the corresponding FE mesh result is available.

For the sake of illustration, the elasticity modulus of the car-door structure is assumed as the Gaussian random field with the exponential covariance model as follows:

$$\mathrm{Cov}(x, y; x', y') = \sigma_E^2(x, y) \exp\left(-\frac{|x - x'|}{\delta_x} - \frac{|y - y'|}{\delta_y}\right), \quad \text{as } \forall x, x', y, y' \in \Omega. \tag{10}$$

Herein, the correlation length parameters in the x- and y-dimension are given as $\delta_x = \delta_y = 1.0\,\mathrm{m}$. Note that the mean-value function is assumed as homogeneous; that is, $\mu_E(x, y) = 2.068 \times 10^5$ MPa. Given the coefficient of variation (COV) 20%, the standard deviation function is defined as $\sigma_E(x, y) = 0.2 \times \mu_E(x, y)$. Based on the FE mesh result of the car-door structure in Figure 1(b), the high-order polynomial-based Rize-Galerkin approach is used to determine numerical results for the eigenvalues and eigenfunctions of the car-door structure.

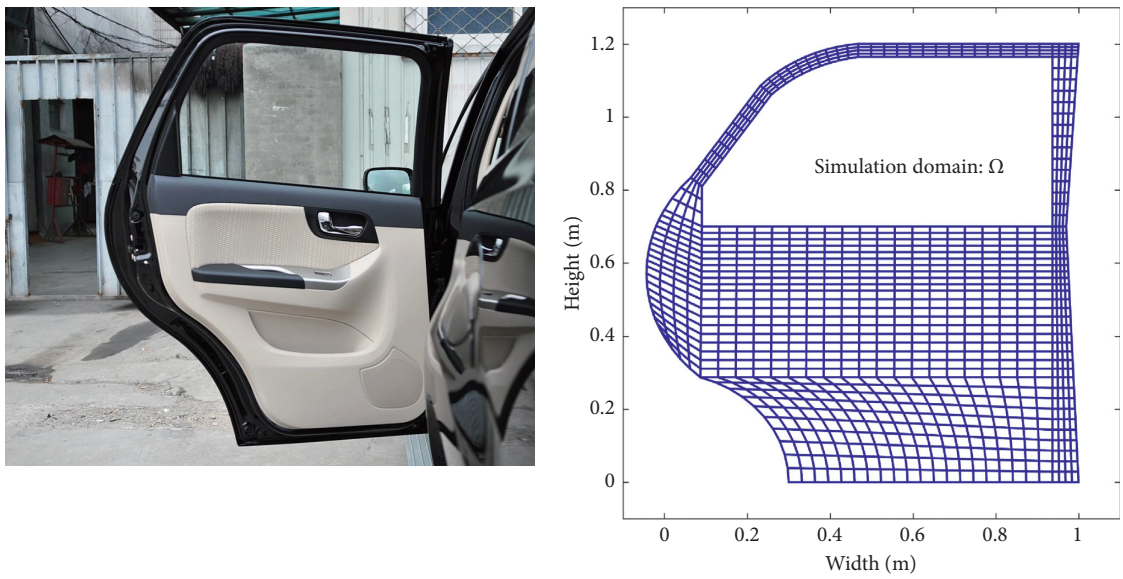

(a) (b)

Figure 1: An illustrative model for random field simulation of the car-door structure. (a) The physical model. (b) Simulation domain and mesh result.

Figure 2 first presents numerical results for eigenvalues of the exponential covariance model, whereas the corresponding results for the first-eight orders of the two-dimensional eigenfunction are depicted in Figure 3. Note that the eigenpair result $\{\lambda_i, \phi_i(x, y)\}$ is no long analytically available for the car-door structure due to its noncanonical simulation region. The tensor-based approximation approach, therefore, is not applicable to simulate the multivariate material random field in this paper.

Once numerical results for the eigenpair are available, numerical realizations of the elastic modulus random field can be generated as

$$\widehat{H}_E(x, y; \boldsymbol{\xi}) \approx \mu_E(x, y) + \sum_{i=1}^{M} \sqrt{\lambda_i}\xi_i\phi_i(x, y), \tag{11}$$

where the truncation order parameter is given as $M = 10$ in subsequent simulations.

Four realizations of the elastic modulus random field are presented in Figure 4. For the sake of illustration, they are randomly selected from totally 10^4 stochastic realizations of the material random field. To implement the Monte-Carlo simulation (MCS) of the material random field, 10^4 samples of the standard Gaussian variables $\xi_i (i = 1, \ldots, M)$ in equation (11) are first digitally generated. Substituting for the corresponding results of the eigenvalues the eigenfunctions in Figures 2 and 3, equation (11) is able to determine the corresponding sample of the elastic modulus random field in conjunction with the truncation order parameter $M = 10$.

It is observed that numerical realizations of the elastic modulus random field are continuously varied around the mean value 2.068×10^5 MPa within the whole simulation domain $(x, y) \in \Omega$, rather than being deterministically fixed as a constant value in conventional formations. With this

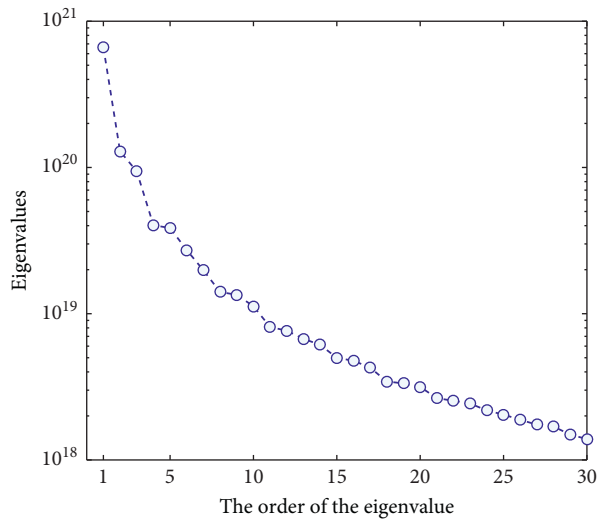

Figure 2: Numerical results for eigenvalues $\lambda_i (i = 1, \ldots, 30)$ of the elastic modulus random field.

spatially varied material uncertainty, structural response quantities, for example, the first-order natural frequency and the lateral stiffness coefficient, become random variables. This motivates the robust design of the car-door structure to simultaneously optimize the performance indicator and minimize the response variance as follows.

Figure 5 further presents relative errors for the mean and the standard deviation functions of the simulated random field, which are generally less than 0.5% and 6.0%, respectively, compared to the benchmark result provided by the MCS method with 10^4 samples. This implies the utility of the truncation parameter $M = 10$ is able to include the majority of input uncertainties for uncertainty simulation of the car-door structure. Similar results for the mass density random

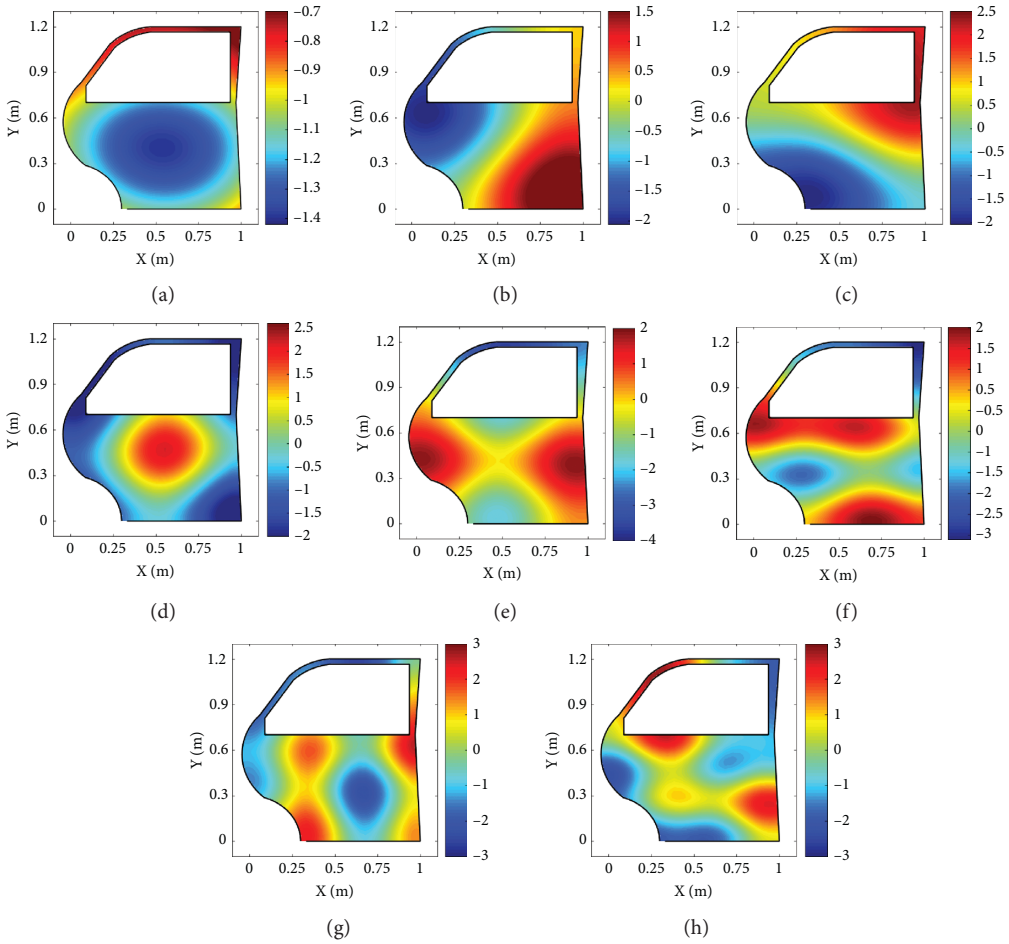

Figure 3: Numerical results for eigenfunctions $\widehat{\phi}_i(x, y)$ $(i = 1, \ldots, 8)$ of the car-door structure based on the exponential covariance mode: the first-eight orders (a~h) of the eigenfunction results.

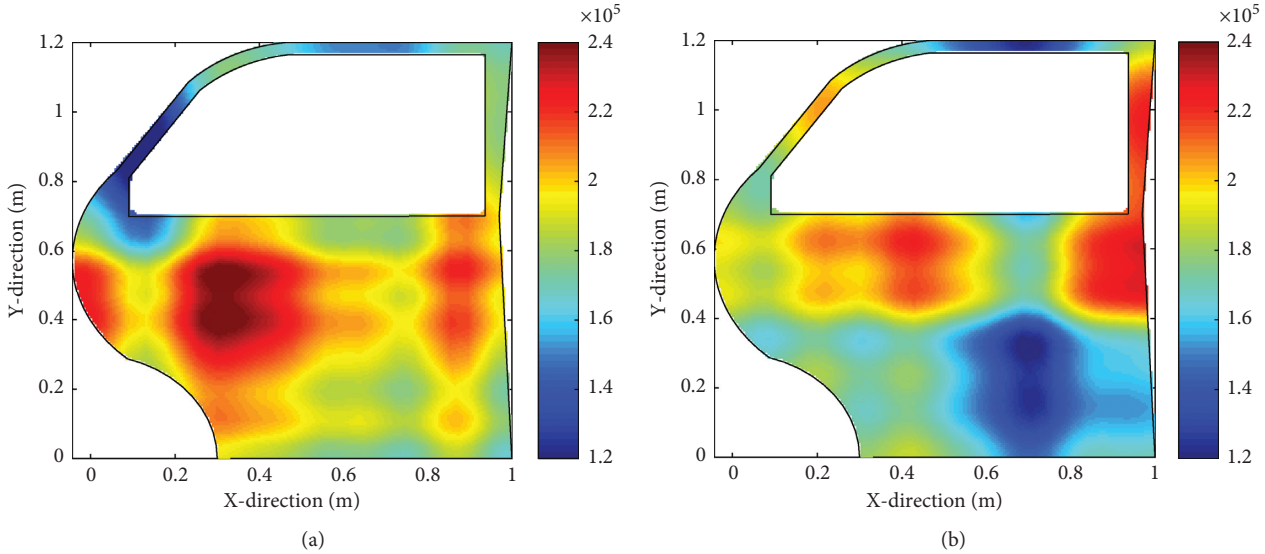

Figure 4: Continued.

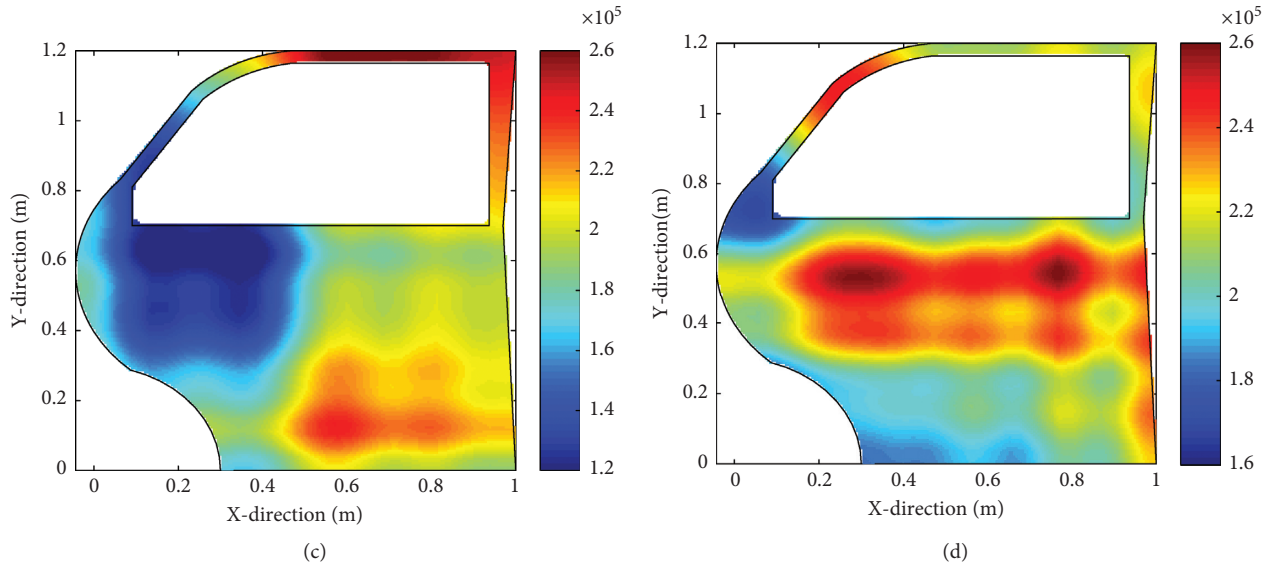

Figure 4: Four realizations (a~d) of the elasticity random field based on the truncation parameter $M = 10$ (unit: MPa).

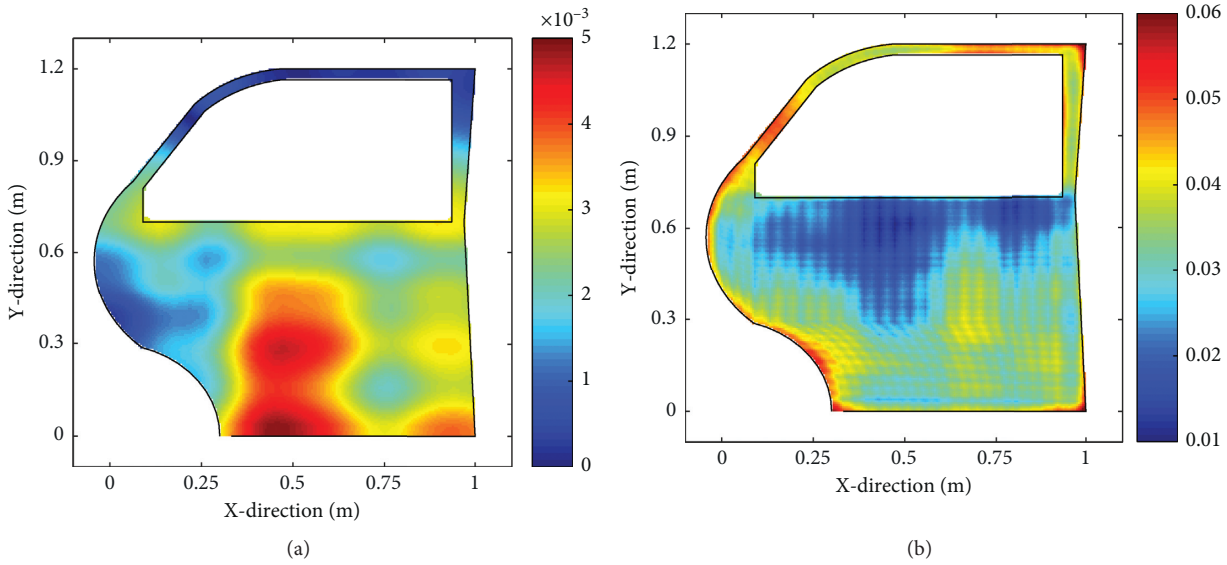

Figure 5: The mean value and the standard deviation errors for the simulation results of the elasticity random field. (a) Relative error for the mean-value function. (b) Relative error for the standard deviation.

field are determined, yet they are omitted here for the sake of brevity. This has verified the applicability of the K-L expansion method for digital simulations of the structural material random fields, and the corresponding stochastic FE model is further derived as follows.

3. Stochastic Finite-Element Model of the Car-Door Structure

Rather than being assumed as deterministic constants, the elastic modulus and the mass density of the car-door structure are further modelled via the random field theory. The utility of the K-L expansion method can represent the material random field by means of a limited number of random variables. Due to this spatially varied material property, uncertain simulation of the car-door structure requires stochastic finite-element models. In this regard, the Mindlin plate theory is first presented for deterministic FE simulation of the car-door structure, whereas stochastic stiffness and mass formulations are further derived to account for the spatially varied material uncertainties. This determines a stochastic FE model for uncertainty analysis of the car-door structure.

3.1. The Mindlin Plate Theory. Following the Mindlin plate theory, the general displacement for the car-door structure can be represented as [29]

$$\begin{cases} u(x,y) = z(x,y)\theta_x(x,y) = z(x,y)\dfrac{\partial w(x,y)}{\partial x}, \\ v(x,y) = z(x,y)\theta_y(x,y) = z(x,y)\dfrac{\partial w(x,y)}{\partial y}, \\ w(x,y) = w(x,y), \end{cases} \tag{12}$$

where u, v, and w denote displacements in the x-, y-, and the z-direction, respectively, whereas θ_x and θ_y represent the corresponding rotation angles as a reference to the neutral surface of the x-z and y-z planes, respectively.

Given the shape function $\mathbf{N}(x,y)$ for the Q4 element, the structural displacement vector can be further interpolated as

$$\begin{cases} w(x,y) = \sum_i N_i(x,y) w_i(x,y), \\ \theta_x(x,y) = \sum_i N_i(x,y)\theta_x(x,y), \\ \theta_y(x,y) = \sum_i N_i(x,y)\theta_y(x,y). \end{cases} \tag{13}$$

Herein, $w_i(x,y)$, $\theta_{xi}(x,y)$, and $\theta_{yi}(x,y)$ denote the displacement components at an ith node of the FE mesh result.

Following the linear stress-strain relation, the stress vector is expressed as

$$\boldsymbol{\sigma} = \mathbf{D}\boldsymbol{\varepsilon}, \tag{14}$$

where $\sigma = [\sigma_x, \sigma_y \gamma_{xy}, \gamma_{xz}, \gamma_{yz},]^T$ and $\varepsilon = [\varepsilon_x, \varepsilon_y \varepsilon_{xy}, \varepsilon_{xz}, \varepsilon_{yz},]^T$ denote the stress and strain tensors, respectively, whereas the matrix $\mathbf{D}$ is given in a diagonal form as

$$\mathbf{D} = \begin{pmatrix} \mathbf{D}_b & \mathbf{0} \\ \mathbf{0} & \mathbf{D}_s \end{pmatrix}. \tag{15}$$

Herein, the bending and shearing matrices are

$$\mathbf{D}_b = \frac{E}{1-\nu^2}\begin{pmatrix} 1 & \nu & 0 \\ \nu & 1 & 0 \\ 0 & 0 & \dfrac{1-\nu}{2} \end{pmatrix}, \qquad \mathbf{D}_s = \frac{E}{2(1+\nu)}\begin{pmatrix} 1 & 0 \\ 0 & 1 \end{pmatrix}. \tag{16}$$

This determines the stiffness matrix for an element of the FE model as

$$\mathbf{K}_e = \frac{h^3}{12}\iint_{\Omega_e} \mathbf{B}_b^{\mathrm{T}}\mathbf{D}_b\mathbf{B}_b \mathrm{d}x\mathrm{d}y + \alpha h \iint_{\Omega_e} \mathbf{B}_s^{\mathrm{T}}\mathbf{D}_s\mathbf{B}_s \mathrm{d}x\mathrm{d}y. \tag{17}$$

Note that Ω_e defines the element of representing the car-door structure, whereas $\alpha = (5/6)$ represents the correction factor associated with the thickness parameter h. Note that the strain matrices $\mathbf{B}_b$ and $\mathbf{B}_s$ are generally defined by partial derivatives of $(\partial N_i(x,y)/\partial x)$ and $(\partial N_i(x,y)/\partial y)$ of the shape function [30].

Similarly, the mass matrix is formulated as

$$\mathbf{M}_e = \iint_{\Omega_e} \rho \mathbf{N}^T \mathrm{diag}\left[h, \frac{h^3}{12}, \frac{h^3}{12}\right]\mathbf{N}\mathrm{d}x\mathrm{d}y, \tag{18}$$

where the two-dimensional integration can be exactly evaluated via the three-order Gauss-Legendre quadrature [30].

Once spatially varied mass and density random fields are considered, the K-L approximation in equation (9) determines the eigenfunction $\widehat{\phi}_i(x,y)$ as high-order polynomials. Therefore, a high-order Gauss-quadrature scheme is required for numerical evaluation of the mass and the stiffness matrix integrals. Besides, the finite-element formulation is derived via the standard Mindlin plate theory [31], and other advanced plate theories can be alternatively used. Once an ordinary FE model is available, a similar stochastic simulation model can be developed as follows for uncertainty simulation of the car-door structure with spatially varied material uncertainties.

3.2. The Stochastic Finite-Element Model. Following the random field simulation procedure presented in Section 2.2, the elastic modulus and the mass density of the car-door structure are realized as spatially varied input uncertainties. The corresponding stiffness and mass matrices of the FE model become spatially dependent within the whole simulation domain. This derives the stochastic FE model as follows.

Following the K-L approximation result, numerical realizations of the elastic modulus and the mass density are given as

$$\begin{cases} \widehat{H}_E(x,y;\boldsymbol{\xi}) \approx \mu_E(x,y) + \sum_{i=1}^{M} \sqrt{\widehat{\lambda}_{Ei}}\,\widehat{\phi}_{Ei}(x,y)\xi_{Ei}, \\ \widehat{H}_\rho(x,y;\boldsymbol{\xi}) \approx \mu_\rho(x,y) + \sum_{i=1}^{M} \sqrt{\widehat{\lambda}_{\rho i}}\,\widehat{\phi}_{\rho i}(x,y)\xi_{\rho i}. \end{cases} \tag{19}$$

Substituting for the uncertain material property, the matrix D in equation (14) is further realized as

$$\mathbf{D}_b(x,y;\boldsymbol{\xi}) = \frac{\widehat{H}_E(x,y;\boldsymbol{\xi})}{1-\nu^2}\begin{pmatrix} 1 & \nu & 0 \\ \nu & 1 & 0 \\ 0 & 0 & \dfrac{1-\nu}{2} \end{pmatrix}, \qquad \mathbf{D}_s(x,y;\boldsymbol{\xi}) = \begin{pmatrix} \dfrac{\widehat{H}_E(x,y;\boldsymbol{\xi})}{2(1+\nu)} & 0 \\ 0 & \dfrac{\widehat{H}_E(x,y;\boldsymbol{\xi})}{2(1+\nu)} \end{pmatrix}. \tag{20}$$

This determines the corresponding stiffness matrix similar to the deterministic result in equation (17) as

$$\mathbf{K}_{\mathrm{e}}(x,y;\boldsymbol{\xi}) = \frac{h^3}{12}\iint_{\Omega_e} \mathbf{B}_b^T\mathbf{D}_b(x,y;\boldsymbol{\xi})\mathbf{B}_b \mathrm{d}x\mathrm{d}y + \alpha h \iint_{\Omega_e} \mathbf{B}_s^T\mathbf{D}_s(x,y;\boldsymbol{\xi})\mathbf{B}_s \mathrm{d}x\mathrm{d}y, \tag{21}$$

which becomes spastically varied due to random factors ξ_i and eigenfunctions $\widehat{\phi}_{Ei}(x, y)$ $(i = 1, \ldots, M)$.

Similarly, the mass matrix that accounts for the material random field is given as

$$\mathrm{M}_e(x, y; \boldsymbol{\xi}) = \iint_{\Omega_e} \widehat{H}_\rho(x, y; \boldsymbol{\xi}) \mathbf{N}^T(x, y) \cdot \mathrm{diag}\left[h, \frac{h^3}{12}, \frac{h^3}{12}\right] \mathbf{N}(x, y) \mathrm{d}x\mathrm{d}y. \tag{22}$$

Substituting for the mass density $\widehat{H}_\rho(x, y; \xi)$ result, the stochastic mass matrix is finally realized as

$$\begin{aligned} \mathrm{M}_e(x, y; \boldsymbol{\xi}) = {} & \iint_{\Omega_e} \mu_\rho(x, y) \mathbf{N}^T(x, y) \mathrm{diag}\left[h, \frac{h^3}{12}, \frac{h^3}{12}\right] \\ & \cdot \mathbf{N}(x, y) \mathrm{d}x\mathrm{d}y + \sum_{i=1}^{M} \sqrt{\widehat{\lambda}_{\rho i}} \xi_{\rho i} \times \\ & \cdot \iint_{\Omega_e} \widehat{\phi}_{\rho i}(x, y) \mathbf{N}^T(x, y) \mathrm{diag}\left[h, \frac{h^3}{12}, \frac{h^3}{12}\right] \\ & \cdot \mathbf{N}(x, y) \mathrm{d}x\mathrm{d}y. \end{aligned} \tag{23}$$

Compared to the deterministic result in equation (18), an introduction of the spatially varied material uncertainties results in high-order integrals with respect to the mean-value function $\mu(x, y)$ and eigenfunctions $\widehat{\phi}_{\rho i}(x, y)$. Note that $\mu(x, y)$ is assumed to be constant for a homogeneous random field in this paper, whereas approximation results for $\widehat{\phi}_{\rho i}(x, y)$ in Figure 3 require high-order polynomials. Therefore, a high-order Gaussian quadrature scheme is necessary for a reliable result of $\mathbf{K}_e(x, y; \xi)$ and $\mathbf{M}_e(x, y; \xi)$ in reality.

Given the isotropic transform of the shape function $\mathbf{N}(x, y)$, the Gauss-Legendre quadrature is used to evaluate the stochastic stiffness and mass matrices. This further determined the global FE model for uncertainty analysis of the car-door structure:

$$\begin{aligned} \mathbf{K}(x, y; \boldsymbol{\xi}) &= \sum_e \mathbf{T}_e \mathbf{K}_e(x, y; \boldsymbol{\xi}) \mathbf{T}_e \mathbf{M}(x, y; \boldsymbol{\xi}) \\ &= \sum_e \mathbf{T}_e \mathbf{M}_e(x, y; \boldsymbol{\xi}) \mathbf{T}_e. \end{aligned} \tag{24}$$

Herein, $\mathbf{T}_e$ represents the coordinate transformation matrix, whereas $\sum_e$ denotes the procedure to assembly all element results together towards the global matrix.

In summary, the stochastic simulation of the car-door structure with spatially varied material uncertainties includes the representation of material random fields via the K-L expansion in Section 2.1, the simulation of the elastic modulus and the mass random fields in Section 2.2, the derivation of stochastic stiffness and mass matrices in equation (21) and (23), and the formulation of stochastic FE models via equation (24).

To demonstrate numerical applications of the presented stochastic FE model for uncertainty simulation of the car-door structure, average models for the elastic modulus and the mass density are constantly assumed as

$$\begin{aligned} \mu_E(x, y) &= 2.068 \times 10^5 \text{ MPa}, \\ \mu_\rho(x, y) &= 7.9 \times 10^3 \text{ kg/m}^3. \end{aligned} \tag{25}$$

Given the coefficient of variation (COV) as 20%, the standard deviation function becomes $\sigma(x, y) = 0.2 \times \mu(x, y)$.

The K-L expansion with the truncation parameter $M = 10$ is first used to simulate the stochastic material property as shown in Figure 4. Then, a sample of the standard Gaussian random variables ξ_{Ei} and $\xi_{\rho i}$ $(i = 1, \ldots, 10)$ is digitally generated to realize the stiffness and mass matrices, and a solution of the general eigenvalue problem determines the corresponding sample of the structural natural frequency.

Repeating this simulation procedure 10^4 times, a collection of all samples allows one to determine an estimation of the mean-value result for the mode shape as shown in Figure 6. Note that the outer boundary of the car-door structure is fully fixed to mimic the closed-door scenario for the natural frequency analysis. In addition, the empirical probability distribution for the first-order natural frequency of the car-door structure is depicted as shown in Figure 7, which has been closely fitted by the Gaussian distribution.

To account for the stiffness characteristic of the car-door structure, the lateral stiffness coefficient is defined as the ratio between the applied force at the door-handle position and the maximal structural deflection. Herein, the applied force is deterministically assumed as 500 N. Therefore, a solution of the equation $\mathbf{K}(x, y; \xi)\mathbf{U}(x, y; \xi) = \mathbf{Q}$ determines the deflection $\mathbf{U}(x, y; \xi)$ and the corresponding sample of the lateral stiffness coefficient.

Figure 8 demonstrates the empirical distribution result of the lateral stiffness coefficient based on 10^{-4} samples of the elastic modulus random field. It is observed that the natural frequency and the lateral stiffness coefficient become random variables after taking into account the spatially varied material uncertainties. This motivates the robust design optimization of the uncertain car-door structure to optimize the performance indicator and simultaneously minimize the response variance as follows.

4. Robust Design Optimization of the Car-Door Structure

This section considers the robust design optimization (RDO) of the car-door structure with spatially varied material uncertainties. To begin with, the multiobjective design functions in terms of the lightweight indicator, the first-order natural frequency, and the lateral stiffness coefficient are formulated. To overcome the computational demanding cost associated with the uncertainty analysis, a polynomial-based regression model is proposed to mimic the true performance function. Together with the probability-based constraint on the structural safety level, this finalizes an effective procedure for the robust design optimization of car-door structures with spatially varied material properties.

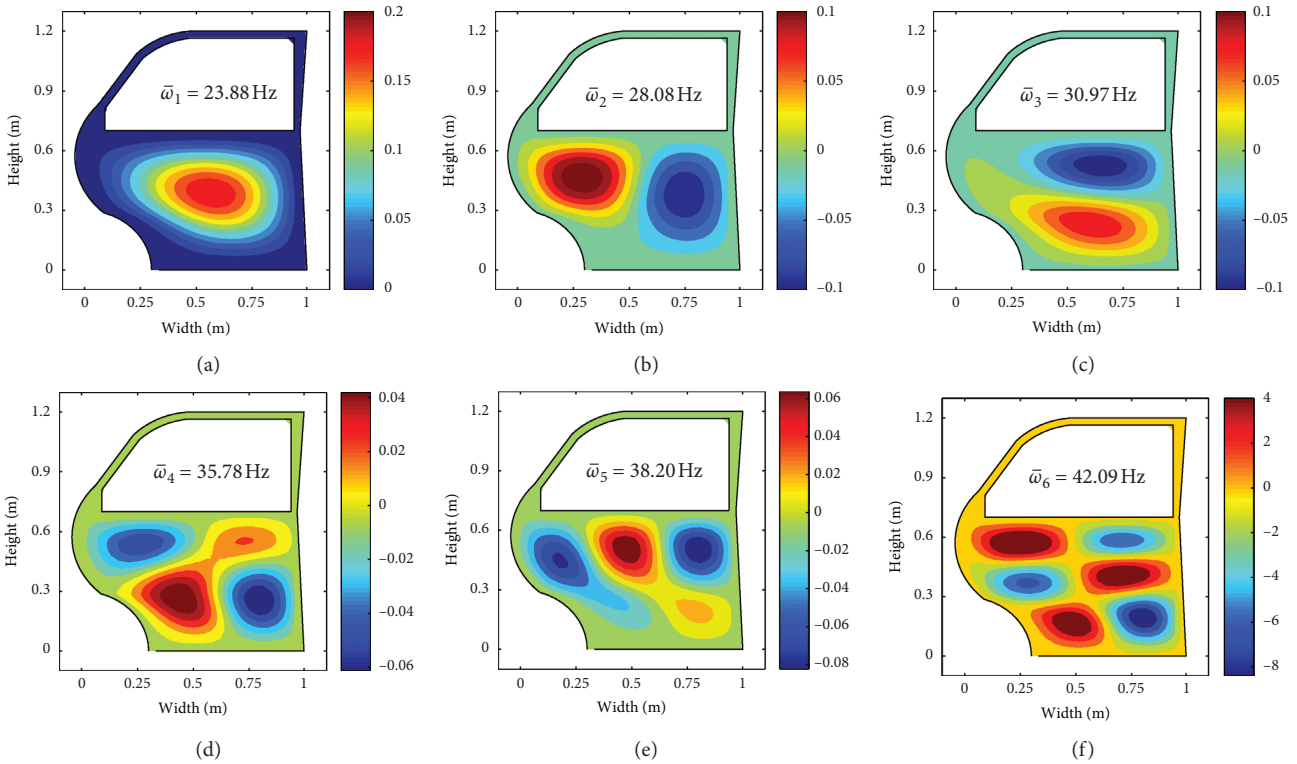

FIGURE 6: Mean-value results for the first-six orders of the structural natural frequency: from (a) to (g).

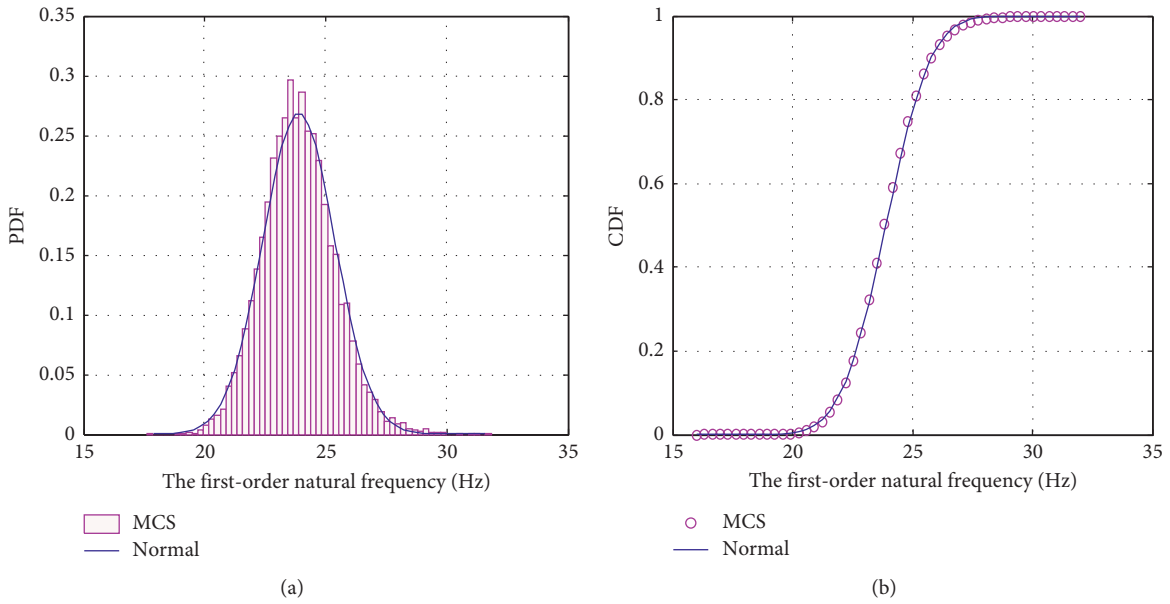

FIGURE 7: The empirical probability distribution for the first-order nature frequency of the car-door structure with spatially varying material properties. (a) The probability density function. (b) The cumulative distribution function.

4.1. The Robust Performance Function. The performance indicators, for example, the first-order natural frequency, the total weight, and the lateral stiffness coefficient, are directly linked with spatially varied material uncertainties of the car-door structure. This is modelled via a stochastic FE formulation based on the Mindlin plate theory. In this respect, the proposed approach can be extended to other plate theories for uncertainty analysis and robust design optimization of the car-door structure.

Due to the input material uncertainties, performance indicators of the car-door structure become random variables. To achieve the robust design optimization, the

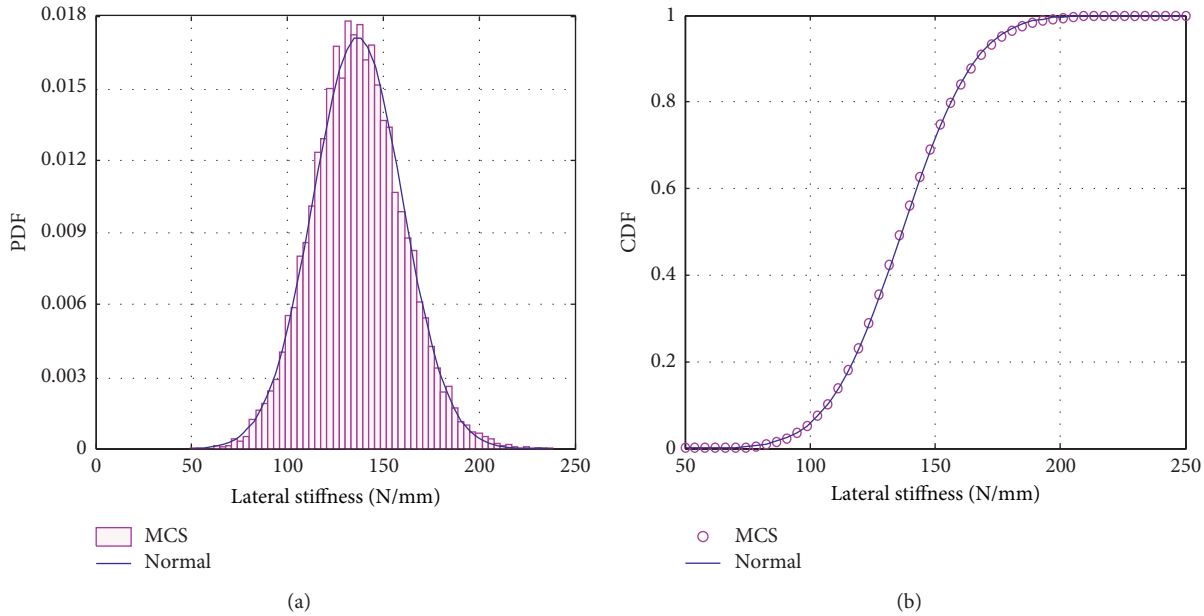

FIGURE 8: The empirical probability distribution for the lateral stiffness coefficient of the car-door structure with spatially varying material properties. (a) The probability density function. (b) The cumulative distribution function.

objective function is usually defined via the average performance $\mu_Y(\mathbf{t})$ and the variance $\sigma_Y^2(\mathbf{t})$. Therefore, three types of the robust design model have been considered in the literature [32]:

(1) Nominal-the-best:

$$F\left(\mu_Y, \sigma_Y^2; \boldsymbol{\xi}, \mathbf{t}\right) = \delta_1\left(\frac{\mu_Y - y_{\text{target}}}{\mu_0 - y_0}\right)^2 + \delta_2\left(\frac{\sigma_Y}{\sigma_0}\right)^2. \quad (26)$$

(i) Herein, y_{target} and y_0 are the target and the initial values of the performance indicator $Y(\mathbf{t}, \xi)$, respectively, and $\delta_1 \in [0,1]$ and $\delta_2 \in [0,1]$ are weights with the relation $\delta_1 + \delta_2 = 1$. To reduce the dimensionality of the mean and the variance objectives, each term has to be normalized by the initial design results μ_0 and σ_0.

(2) Smaller-the-best:

$$F\left(\mu_Y, \sigma_Y^2; \boldsymbol{\xi}, \mathbf{t}\right) = \delta_1\left(\frac{\mu_Y}{\mu_0}\right)^2 + \delta_2\left(\frac{\sigma_Y}{\sigma_0}\right)^2. \quad (27)$$

(3) Largest-the-best:

$$F\left(\mu_Y, \sigma_Y^2; \boldsymbol{\xi}, \mathbf{t}\right) = \delta_1\left(\frac{\mu_0}{\mu_Y}\right)^2 + \delta_2\left(\frac{\sigma_Y}{\sigma_0}\right)^2. \quad (28)$$

In this paper, the main objective of the design optimization is to maximize the first-order natural frequency and the structural lateral stiffness coefficient and yet minimize the structural total weight and the response variance. This determines the design objective functions as

$$\begin{cases} F_m(\boldsymbol{\xi}, \mathbf{t}) = \delta_{m1}\left(\dfrac{\mu_m(\boldsymbol{\xi}, \mathbf{t})}{\mu_m^0(\boldsymbol{\xi}, \mathbf{t})}\right) + \delta_{m2}\left(\dfrac{\sigma_m(\boldsymbol{\xi}, \mathbf{t})}{\sigma_m^0(\boldsymbol{\xi}, \mathbf{t})}\right), \\ F_f(\boldsymbol{\xi}, \mathbf{t}) = \delta_{f1}\left(\dfrac{\mu_f^0(\boldsymbol{\xi}, \mathbf{t})}{\mu_f(\boldsymbol{\xi}, \mathbf{t})}\right) + \delta_{f2}\left(\dfrac{\sigma_f(\boldsymbol{\xi}, \mathbf{t})}{\sigma_f^0(\boldsymbol{\xi}, \mathbf{t})}\right), \\ F_s(\boldsymbol{\xi}, \mathbf{t}) = \delta_{s1}\left(\dfrac{\mu_s^0(\boldsymbol{\xi}, \mathbf{t})}{\mu_s(\boldsymbol{\xi}, \mathbf{t})}\right) + \delta_{s2}\left(\dfrac{\sigma_s(\boldsymbol{\xi}, \mathbf{t})}{\sigma_s^0(\boldsymbol{\xi}, \mathbf{t})}\right). \end{cases} \quad (29)$$

Herein, symbols with the subscript "0" represent the nominal value, whereas $\mu(\cdot)$ and $\sigma(\cdot)$ define the mean value and the standard variation of the performance indicator. Together with weighting coefficients $\delta(\cdot)$, the mass, the natural frequency, and the stiffness functions are defined for the robust-based design optimization.

Specifically, the door structure is manufactured as the tailor rolled blank with different thickness values, that is, the hinge reinforcement panel t_1, the window frame t_2, the lock reinforcement panel t_3, the window reinforcement panel t_4, and the interior and outer panels t_5 and t_6 [33]. Note that the initial values of the design variable are assumed as $\mathbf{t}_0 = [1.5, 2.4, 0.8, 1.2, 1.0, 1.7]^T$ (unit: mm). Together with the lower and upper design limits $\mathbf{t}^L = [1.0, 1.8, 0.5, 0.7, 0.5, 1.0]^T$ and $\mathbf{t}^U = [2.5, 3.0, 1.5, 2.0, 1.5, 2.5]^T$, the parameters will be used for design optimizations of the car-door structure.

Following the stochastic simulation procedure of the door structure, the mean value of the total weight, the first-order natural frequency, and the lateral stiffness coefficient are estimated as 6.66 kg, 23.88 Hz, and 136.01 N/mm, respectively, whereas the corresponding standard deviation results are given as 1.03 kg, 2.38 Hz, and 22.57 N/mm. To

efficiently realize the robust design optimization, a polynomial-based response surface method is determined as follows to reduce the embedded computational cost for probabilistic simulations.

4.2. The Response Surface Model. The performance indicators defined in equation (29) are formulated by standard Gaussian random variables ξ and design parameters $\mathbf{t} = [t_1, \ldots, t_6]^T$. The corresponding design iterations need to recursively run the stochastic FE model for the mean value and the variance results of the design function. To reduce the total amount of the computational cost, a polynomial-based response surface model is used to mimic the true performance function of the car-door structure as follows.

The polynomial-based response surface model (p-RSM) has been widely used to represent complex input-output relations in engineering reality. However, the total number of samples for a reliable predictor is positively proportional to the highest-order of the polynomial function, which motivates us to use quadratic p-RSM including mixed terms in this paper [34–36]:

$$y = a + \sum_{i=1}^{m} b_i u_i + \sum_{i=1}^{m} c_i u_i^2 + \sum_{i=1}^{m-1} \sum_{j>i}^{m} d_{ij} u_i u_j + \epsilon_{\text{err}}. \tag{30}$$

Herein, the variable y represents a performance indicator, that is, the structural weight, the first-order natural frequency, and the lateral stiffness coefficient, whereas the vector $\mathbf{u}$ contains all design variables t_i and the standard Gaussian variables ξ_i due to the discretization result of the material random field. Totally, $l = 2m + 6\,(m = 10)$ variables are finally involved to develop the response surface model.

Or in a matrix form, the second-order p-RSM model can be expressed as

$$y = \mathbf{u}^T \boldsymbol{\beta} + \epsilon_{\text{err}}. \tag{31}$$

To determine the regression vector β, totally $p = 3 \times (2m + 6)$ low-discrepancy realizations of the structural performance indicator are gathered as the training dataset $\mathbf{y} = [y_1, \ldots, y_p]^T$:

$$\Xi = \begin{bmatrix} 1 & u_{11} & \cdots & u_{1l}^2 & \cdots & u_{1(l-1)}u_{1l} \\ 1 & u_{21} & \cdots & u_{2l}^2 & \cdots & u_{2(l-1)}u_{2l} \\ \vdots & \ddots & \ddots & \vdots & \ddots & \vdots \\ 1 & u_{p1} & \cdots & u_{pl}^2 & \cdots & u_{p(l-1)}u_{pl} \end{bmatrix}_{p \times q}, \tag{32}$$

where the parameter q is defined as $(l + 1)(l + 2)/2$.

This determines the regression coefficients in equation (31) as

$$\widehat{\beta} = \left(\Xi^{\mathrm{T}} \Xi\right)^{-1} \Xi^{\mathrm{T}} \mathbf{y}, \tag{33}$$

as well as the covariance matrix

$$\mathrm{Cov}(\widehat{\beta}) = \sigma_{\text{err}}^2 \left(\Xi^{\mathrm{T}} \Xi\right)^{-1}. \tag{34}$$

Here, the symbol σ_{err}^2 denotes the global variance of the residual error ϵ_{err}, and its unbiased estimator is given as

$$\widehat{\sigma}_{\text{err}}^2 = \frac{z^T \left(\mathbf{I}_p - \mathbf{H}\right) \mathbf{y}}{q - p}, \tag{35}$$

where $\mathbf{I}_p$ denotes a $p \times p$ identity matrix and $\mathbf{H} = \Xi(\Xi^T \Xi)^{-1} \Xi^T$.

Once the training matrix Ξ defined in equation (32) and the corresponding performance samples $\mathbf{y}$ are available, the minimization of the residual errors allows one to derive the p-RSM as

$$\widehat{y}(\boldsymbol{\xi}, \mathbf{t}) = \mathbf{u}^T \widehat{\beta}, \quad \text{where } \mathbf{u} = \left[\mathbf{t}^T, \boldsymbol{\xi}^T\right]^T, \tag{36}$$

which is used to mimic the true but computationally intensive stochastic finite-element response of the car-door structure.

Figure 9 presents the polynomial-based surrogate model for the structural weight $\mathscr{M}(\xi, \mathbf{t})$, the first-order natural frequency $\mathscr{F}(\xi, \mathbf{t})$, and the lateral stiffness coefficient $\mathscr{S}(\xi, \mathbf{t})$. As a reference to the benchmark result provided by the stochastic finite-element simulation, the numerical accuracy of the surrogate model $\widehat{y}$ can be evaluated by the root-of-mean-square error (RMSE):

$$\mathrm{RMSE} \coloneqq \frac{1}{m\overline{y}} \sqrt{\sum_{i=1}^{m} (y_i - \widehat{y}_i)^2}, \tag{37}$$

where the mean value of the prediction result is defined as $\overline{y} = (1/m) \sum_{i=1}^{m} y_i$.

Results for the RMSE in Table 1 have shown the high accuracy of the p-RSM for reliable prediction results. The small statistical error $(\mathrm{RMSE} \leq 1.956 \times 10^{-3})$ has validated the applicability of the quadratic surrogate model for design optimization of the uncertain car-door structure.

Therefore, a mathematical model for the probability-based robust design optimization of the car-door structure is finally formulated as

$$\begin{cases} \text{Find}: t^* = \left[t_1^*, \ldots, t_6^*\right]^T \\ \min\{F_m(\boldsymbol{\xi}, \mathbf{t})\} \cap \max\left\{F_f(\boldsymbol{\xi}, \mathbf{t})\right\} \cap \max\{F_s(\boldsymbol{\xi}, \mathbf{t})\} \\ \text{s.t. } t_i^L \leq t_i \leq t_i^U \\ \Pr\left[\mathscr{F}(\boldsymbol{\xi}, \mathbf{t}) \geq f_0\right] \geq P_1 \\ \Pr\left[S(\boldsymbol{\xi}, \mathbf{t}) \geq s_0\right] \geq P_2. \end{cases} \tag{38}$$

Herein, $F_{(\cdot)}(\xi, \mathbf{t})$ denotes {design} objectives listed in equation (29), whereas the weighting coefficients are given as 0.5. This implies that the mean and variance of the performance function have been equivalently treated for the robust design optimization. Specifically, the operator $\Pr(\cdot)$ evaluates the probability of a performance indicator over its design limit. Together with the targeted probability $P_i\,(i = 1, 2)$, this allows one to determine the corresponding design result associated with the targeted safety level, for example, 90% or 95% in numerical examples.

4.3. Numerical Results for the Design Optimization. The robust design optimization of the car-door structure with

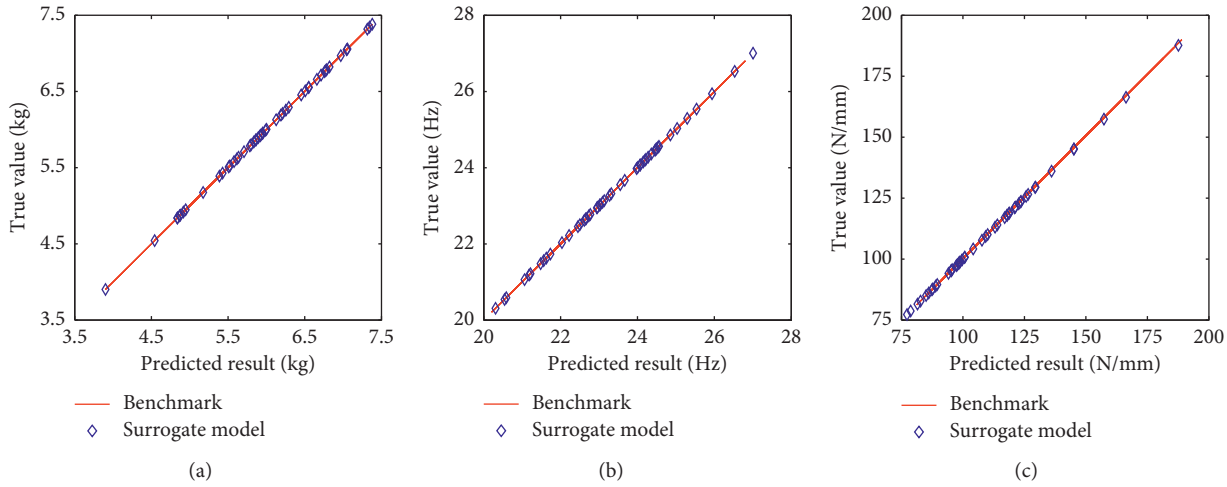

Figure 9: Numerical verification of the response surface model for the performance indicator of the car-door structure. (a) The total weight. (b) The first-order natural frequency. (c) The lateral stiffness coefficient.

Table 1: Results for the RMSE of the polynomial-based response surface model.

	Total weight $\mathscr{M}(\xi, \mathbf{t})$	Natural frequency $\mathscr{F}(\xi, \mathbf{t})$	Lateral stiffness $\mathscr{S}(\xi, \mathbf{t})$
RMSE	2.139×10^{-4}	8.365×10^{-4}	1.956×10^{-3}

spatially varied material properties is numerically realized based on the flowchart depicted in Figure 10. This includes the reproduction of material random field simulation with the truncated K-L expansion in equation (11), the development of the stochastic finite-element model for uncertain mass, stiffness coefficient, and natural frequency analysis in Section 3.2, and the utility of the polynomial-based response surface model to mimic the structural performance indicators in equation (30). Once the robust design optimization model in equation (38) is set up, numerical iteration to optimize design variables is realized with the genetic algorithm in the literature [21].

To begin with, the structural design optimization is considered based on various objectives in equation (29). In this regard, the lightweight design objective has been considered as the priority. Combined with the natural frequency and the lateral stiffness indicators, this determines two design cases for the biobjective design optimization.

Table 2 summarizes the robust design optimization result for the single, bi, and triobjective scenarios. In general, the design optimization is able to simultaneously improve the performance indicator and minimize the response variance. However, the uniobjective design can determine the most optimum result among all investigated scenarios. For instance, the mean value of the lateral stiffness coefficient $\mathscr{S}(\xi, \mathbf{t})$ has been improved from 136.01 N/mm to 145.25 N/mm with an increasing rate 6.79%, whereas the response variance has been significantly minimized over 61.4% (from 508.95 N2/mm^2 to 196.28 N2/mm^2). A small response variance implies the improved robustness to accommodate potential variabilities caused by input material uncertainties. As a comparison, results based on the bi- and triobjective functions are not improved as much as that of the single-objective case. Therefore, the biobjective scenarios, that is, $\min\{F_m(\xi, \mathbf{t})\} \cap \max\{F_f(\xi, \mathbf{t})\}$ and $\min\{F_m(\xi, \mathbf{t})\} \cap \max\{F_s(\xi, \mathbf{t})\}$, will be further investigated in conjunction with various probability-based constraint levels.

To account for the effect of a probability-based constraint on the lightweight design of the uncertain car-door structure, threshold values for the first-order natural frequency and the lateral stiffness coefficient are given as 22 Hz and 123 N/mm, respectively. Following the procedure in equation (38), Table 3 summarizes the corresponding lightweight design result associated with the targeted safety levels 90% and 95%. Note that initial values and design boundaries of the design variable t are similar to those in the foregoing section.

Compared to the initial design result, the mean value of the total mass $\mathscr{M}(\xi, \mathbf{t})$ has been generally minimized for all investigated cases, yet they are all slightly heavier than those provided in Table 2. This is mainly due to additional safety constraints on the first-order natural frequency and the lateral stiffness. To better understand the effect of this safety-related constraint, the Pareto optimum sets for the weight-frequency and the weight-stiffness objectives are determined as follows.

Figure 11 depicts the Pareto result for the weight-frequency and the weight-stiffness biobjective functions in conjunction with the 90% and 95% safety levels. The third performance function, for example, the lateral stiffness coefficient in the weight-frequency case, has been used to define the probability constraint. It is observed that the 95% probability level determines a more conservative result than that of the 90% nonexceeding probability. For instance, a realization of the Pareto optimum set can be determined as

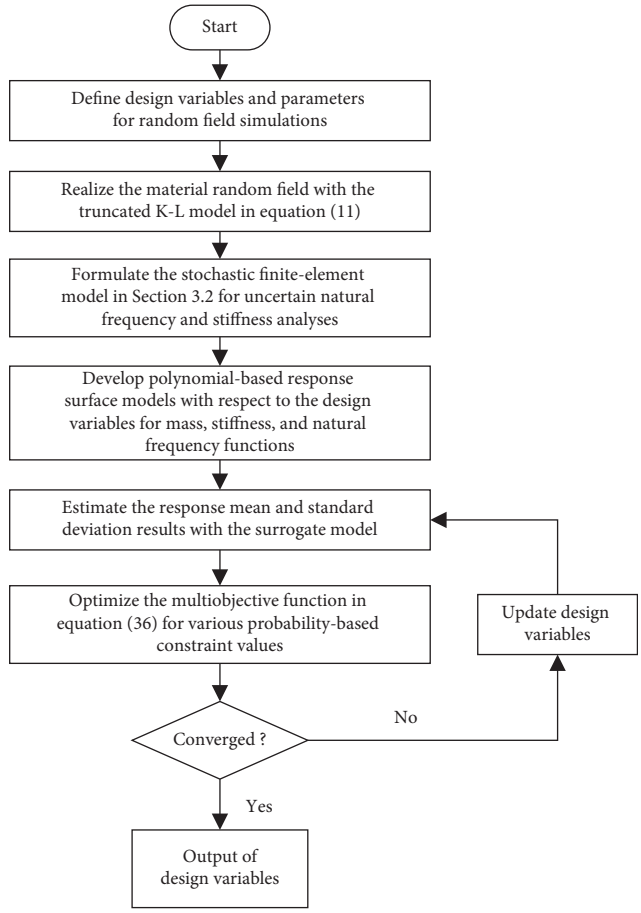

Figure 10: The flowchart for robust design optimization of the car-door structure with spatially varied material properties.

Table 2: Results for the robust design optimization based on various combinations of the objective function.

	Initial result			Uniobjective			Biobjective		Triobjective
	$\mathscr{M}_0$	$\mathscr{F}_0$	$\mathscr{S}_0$	$\mathscr{M}^*$	$\mathscr{F}^*$	$\mathscr{S}^*$	$\mathscr{M}^* \cap \mathscr{F}^*$	$\mathscr{M}^* \cap \mathscr{S}^*$	$\mathscr{M}^* \cap \mathscr{F}^* \cap \mathscr{S}^*$
Mean	6.66	23.88	136.01	4.37	26.04	145.25	5.01, 24.73	4.87, 142.5	5.06, 24.28, 140.25
Std.D	1.03	2.41	22.56	0.51	1.58	14.10	0.61, 1.84	0.57, 15.22	0.63, 1.96, 16.17
COV	15.5%	10.09%	16.58%	10.98%	10.98%	9.70%	12.17%, 7.44%	11.49%, 10.68%	12.45%, 8.07%, 11.53%

Std.D: standard deviation; COV: coefficient of variation.

Table 3: Results for the lightweight design optimization associated with various probability-based constraints.

Probability-based constraint	t_1^*	t_2^*	t_3^*	t_4^*	t_5^*	t_6^*	$\mathscr{M}(\xi, \mathbf{t}^*)$	
							Mean	COV (%)
$\Pr[\mathscr{F}(\xi, \mathbf{t}) \geq f_0] \geq 90\%$	1.4284	1.9427	0.6406	0.7791	0.5985	1.2617	4.9889	9.78
$\Pr[\mathscr{F}(\xi, \mathbf{t}) \geq f_0] \geq 95\%$	1.4531	1.9819	0.6780	0.8121	0.6369	1.3291	5.1712	10.66
$\Pr[\mathscr{S}(\xi, \mathbf{t}) \geq f_0] \geq 90\%$	1.4775	2.1364	0.7385	0.8976	0.7643	1.4917	5.6679	8.91
$\Pr[\mathscr{S}(\xi, \mathbf{t}) \geq f_0] \geq 95\%$	1.4749	2.1245	0.7346	0.9115	0.7585	1.4731	5.8578	10.52

$f_0 = 22$ Hz and $s_0 = 123$ N/mm.

(24 Hz, 5.81 kg) for the 90% safety level, whereas this total weight result will be increased to 7.0 kg for the 95% probability level and the identical natural frequency result. As a comparison, the Pareto curve for the weight-stiffness case is almost identical for the two investigated probability scenarios. In this regard, one can conclude that the first-order natural frequency is more sensitive to the variation of thickness variables than that of the lateral stiffness coefficient.

To investigate the effect of the input variability on the design optimization result, Figure 12 presents the corresponding Pareto optimum set based on various COV values

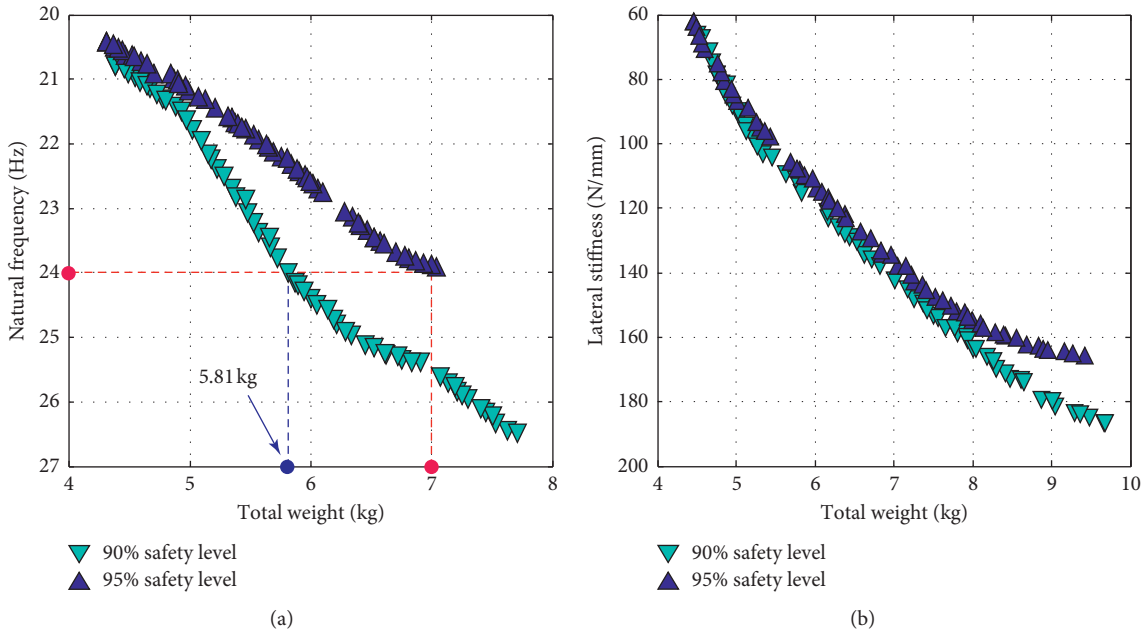

Figure 11: The Pareto results for the weight-frequency and the weight-stiffness biobjective functions of the uncertain car-door structure associated with 90% and 95% probability-based constraints. (a) The weight-frequency biobjective function. (b) The weight-frequency biobjective function.

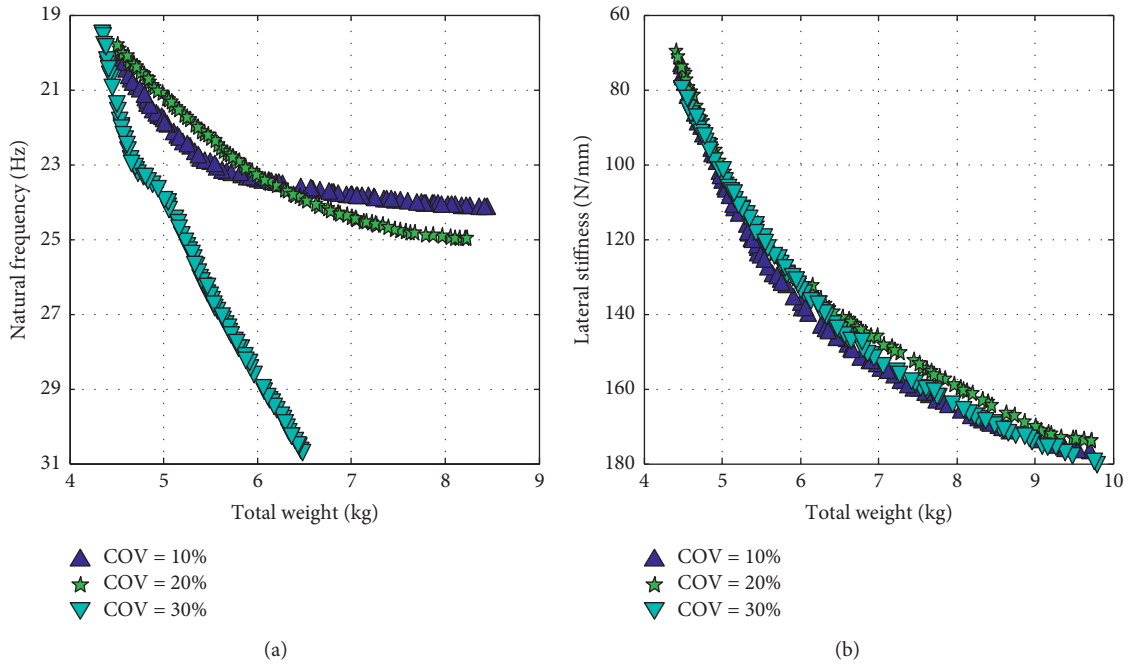

Figure 12: The Pareto result for the lightweight design optimization of the car-door structure (the legends indicate the COV values of the material random field). (a) The weight-frequency objective function. (b) The weight-frequency objective function.

of the material random field. In this regard, the COV value of the Exponential covariance model has been assumed to vary from 10% to 30%. Combined with the 95%-based probability constraint, significantly divergent Pareto optimum sets were obtained for the weight-frequency objective function. This has confirmed the large variation of the first-order natural frequency with respect to the COV value of the material random field. This is obvious for the case of COV = 30%, in which a small increase of the structural weight can result in a dramatic increase in the first-order natural frequency. The lateral stiffness coefficient, however, is almost insensitive to the COV value of the material random field. Therefore, the Pareto optimum sets for the weight-stiffness case are almost identical for various COV values. In summary, the

effectiveness of the proposed procedure has been further justified by numerical robust design optimization of the uncertain car-door structure with various COV values of the material random field.

5. Conclusions

This paper presents an effective approach for the robust design optimization of car-door structures with spatially varied material uncertainties. To implement, the Karhunen-Loève expansion method is first used to represent the elastic modulus and the mass density random fields as a few deterministic functions and random variables. Then, a stochastic finite-element model is developed for uncertainty simulation of the car-door structure. To reduce the computational cost for iteratively running the mechanistic model, a polynomial-based surrogate model is developed to predict stochastic responses of the uncertain car-door structure. Combined with various probability-based constraints to address the safety issue, robust design optimization of the uncertain car-door structure is finally realized through the genetic algorithm to search for optimum mean-value performance results and simultaneously minimizing the response variance.

Numerical results have shown that the polynomial-based surrogate model is able to provide reliable prediction results for uncertain response quantities of the uncertain car-door structure, whereas the mean and the variance of the performance function can be generally improved via the proposed robust design model. The 95%-based probability constraint function determines a more conservative result than that of the 90% safety level. The COV value of the covariance model has shown a significant effect on the Pareto optimum set for the first-order natural frequency performance function, whereas results for the weight-stiffness biobjective function are determined almost identical for various input COV levels. This has demonstrated potential applications of the proposed approach for the robust design optimization of uncertain car-door structures with spatially varied material properties.

Data Availability

The simulation data within this submission are available upon request.

Conflicts of Interest

The authors declare that they have no conflicts of interest.

Acknowledgments

The authors would like to acknowledge the Liaoning Provincial Key Research and Development Project (Grant no 2019JH8/10100056) and the National Natural Science Foundation of China (Grant no. 71672117) for financially supporting the research.

References

[1] Y. Jung, S. Lim, J. Kim, and S. Min, "Light weight design of electric bus roof structure using multi-material topology optimisation," *Structural and Multidisciplinary Optimization*, vol. 61, no. 6, pp. 1273–1285, 2020.

[2] P. Sasikumar, R. Suresh, and S. Gupta, "Stochastic model order reduction in uncertainty quantification of composite structures," *Composite Structures*, vol. 128, pp. 21–34, 2015.

[3] P. Kunakorn-ong, K. Ruangjirakit, P. Jongpradist, S. Aimmanee, and Y. Laoonual, "Design and optimization of electric bus monocoque structure consisting of composite materials," *Proceedings of the Institution of Mechanical Engineers, Part C: Journal of Mechanical Engineering Science*, vol. 234, no. 20, pp. 4069–4086, 2020.

[4] F. Lan, J. Chen, and J. Lin, "Comparative analysis for bus side structures and lightweight optimization," *Proceedings of the Institution of Mechanical Engineers, Part D: Journal of Automobile Engineering*, vol. 218, no. 10, pp. 1067–1075, 2004.

[5] W. Zhong, R. Su, L. Gui, and Z. Fan, "Multi-objective topology and sizing optimization of bus body frame," *Structural and Multidisciplinary Optimization*, vol. 54, no. 3, pp. 701–714, 2016.

[6] S. P. Zhu, S. Foletti, and S. Beretta, "Probabilistic framework for multiaxial lcf assessment under material variability," *International Journal of Fatigue*, vol. 103, pp. 371–385, 2017.

[7] H. Fang, C. Gong, H. Su, Y. Zhang, C. Li, and A. Da Ronch, "A gradient-based uncertainty optimization framework utilizing dimensional adaptive polynomial chaos expansion," *Structural and Multidisciplinary Optimization*, vol. 59, no. 4, pp. 1199–1219, 2019.

[8] X. Zhang, L. Wang, and J. D. Sørensen, "REIF: a novel active-learning function toward adaptive Kriging surrogate models for structural reliability analysis," *Reliability Engineering & System Safety*, vol. 185, pp. 440–454, 2019.

[9] H. Lu, Z. Zhu, and Y. Zhang, "A hybrid approach for reliability-based robust design optimization of structural systems with dependent failure modes," *Engineering Optimization*, vol. 52, no. 3, pp. 384–404, 2020.

[10] H. Dai and Z. Cao, "A wavelet support vector machine-based neural network metamodel for structural reliability assessment," *Computer-Aided Civil and Infrastructure Engineering*, vol. 32, no. 4, pp. 344–357, 2017.

[11] S.-P. Zhu, B. Keshtegar, M. Bagheri, P. Hao, and N.-T. Trung, "Novel hybrid robust method for uncertain reliability analysis using finite conjugate map," *Computer Methods in Applied Mechanics and Engineering*, vol. 371, Article ID 113309, 2020.

[12] S. P. Zhu, B. Keshtegar, N. T. Trung, Z. M. Yaseen, and D. T. Bui, "Reliability-based structural design optimization: hybridized conjugate mean value approach," in *Engineering with Computers*, pp. 1–14, Springer, Berlin, Germany, 2019.

[13] M. Guedri, A. M. G. Lima, N. Bouhaddi, and D. A. Rade, "Robust design of viscoelastic structures based on stochastic finite element models," *Mechanical Systems and Signal Processing*, vol. 24, no. 1, pp. 59–77, 2010.

[14] F. Li, G. Sun, X. Huang, J. Rong, and Q. Li, "Multiobjective robust optimization for crashworthiness design of foam filled thin-walled structures with random and interval uncertainties," *Engineering Structures*, vol. 88, pp. 111–124, 2015.

[15] G. Sun, X. Song, S. Baek, and Q. Li, "Robust optimization of foam-filled thin-walled structure based on sequential Kriging metamodel," *Structural and Multidisciplinary Optimization*, vol. 49, no. 6, pp. 897–913, 2014.

[16] R. G. Ghanem and P. D. Spanos, *Stochastic Finite Elements: A Spectral Approach*, Springer, Berlin, Germany, 2003.
[17] J. Deng, "Structural reliability analysis for implicit performance function using radial basis function network," *International Journal of Solids and Structures*, vol. 43, no. 11-12, pp. 3255–3291, 2006.
[18] P. Wang, W. Wei, Z. Li, W. Duan, H. Han, and Q. Xie, "A superhydrophobic fluorinated PDMS composite as a wearable strain sensor with excellent mechanical robustness and liquid impalement resistance," *Journal of Materials Chemistry A*, vol. 8, no. 6, pp. 3509–3516, 2020.
[19] G. I. Schuëller and H. J. Pradlwarter, "Benchmark study on reliability estimation in higher dimensions of structural systems - an overview," *Structural Safety*, vol. 29, no. 3, pp. 167–182, 2007.
[20] X. Zhang, L. Wang, and J. D. Sørensen, "AKOIS: an adaptive Kriging oriented importance sampling method for structural system reliability analysis," *Structural Safety*, vol. 82, 2020.
[21] M. Bagheri, B. Keshtegar, S.-P. Zhu, D. Meng, J. A. F. O. Correia, and A. M. P. D. Jesus, "Fuzzy reliability analysis using genetic optimization algorithm combined with adaptive descent chaos control," *ASCE-ASME Journal of Risk and Uncertainty in Engineering Systems, Part A: Civil Engineering*, vol. 6, no. 2, Article ID 04020022, 2020.
[22] C. Zienkiewicz and R. L. Taylor, *·e Finite Element Method: Solid Mechanics*, Butterworth-Heinemann, Oxford, UK, 2000.
[23] F. Gruttmann and W. Wagner, "A stabilized one-point integrated quadrilateral Reissner-Mindlin plate element," *International Journal for Numerical Methods in Engineering*, vol. 61, no. 13, pp. 2273–2295, 2004.
[24] J. N. Reddy, *Theory and Analysis of Elastic Plates and Shells*, CRC Press, Boca Raton, FL, USA, 2006.
[25] Y. Zhou and X. Zhang, "Natural frequency analysis of functionally graded material beams with axially varying stochastic properties," *Applied Mathematical Modelling*, vol. 67, pp. 85–100, 2019.
[26] X. Zhang and M. D. Pandey, "Structural reliability analysis based on the concepts of entropy, fractional moment and dimensional reduction method," *Structural Safety*, vol. 43, no. 3, pp. 28–40, 2013.
[27] K. E. Atkinson, *The Numerical Solution of Integral Equations of the Second Kind*, Cambridge University Press, Cambridge, UK, 1997.
[28] C. C. Li and A. Der Kiureghian, "Optimal discretization of random fields," *Journal of Engineering Mechanics*, vol. 119, no. 6, pp. 1136–1154, 1993.
[29] X. Zhang, Q. Liu, and H. Huang, "Numerical simulation of random fields with a high-order polynomial based Ritz-Galerkin approach," *Probabilistic Engineering Mechanics*, vol. 55, pp. 17–27, 2019.
[30] F. Auricchio and R. L. Taylor, "A shear deformable plate element with an exact thin limit," *Computer Methods in Applied Mechanics and Engineering*, vol. 118, no. 3-4, pp. 393–412, 1994.
[31] R. T. Zienkiewicz and J. Zhu, *The Finite Element Method: Its Basis and Fundamentals*, Elsevier Butterworth-Heinemann, Oxford, UK, 2013.
[32] K.-J. Bathe and E. N. Dvorkin, "A four-node plate bending element based on mindlin/reissner plate theory and a mixed interpolation," *International Journal for Numerical Methods in Engineering*, vol. 21, no. 2, pp. 367–383, 1985.
[33] K. K. Choi, I. Lee, and D. Gorsich, "Dimension reduction method for reliability-based robust design optimization," *Computers & Structures*, vol. 86, no. 13, pp. 1550–1562, 2008.
[34] G. Sun, H. Zhang, J. Fang, G. Li, and Q. Li, "Multi-objective and multi-case reliability-based design optimization for tailor rolled blank (TRB) structures," *Structural and Multidisciplinary Optimization*, vol. 55, no. 5, pp. 1899–1916, 2017.
[35] D. Zhang, N. Zhang, N. Ye, J. Fang, and X. Han, "Hybrid learning algorithm of radial basis function networks for reliability analysis," *IEEE Transactions on Reliability*, pp. 1–14. In press, 2020.
[36] J. Wu, D. Zhang, C. Jiang, X. Han, and Q. Li, "On reliability analysis method through rotational sparse grid nodes," *Mechanical Systems and Signal Processing*, vol. 147, p. 107106, 2021.